Efferocytosis produces a prometastatic landscape during postpartum mammary gland involution

Jamie C. Stanford,[1] Christian Young,[2] Donna Hicks,[1] Philip Owens,[1] Andrew Williams,[1] David B. Vaught,[1] Meghan M. Morrison,[1] Jiyeon Lim,[1] Michelle Williams,[1] Dana M. Brantley-Sieders,[2] Justin M. Balko,[2] Debra Tonetti,[3] H. Shelton Earp III,[4] and Rebecca S. Cook[1,5]

[1]Department of Cancer Biology and [2]Department of Medicine, Vanderbilt University School of Medicine, Nashville, Tennessee, USA. [3]University of Illinois, Chicago, Illinois, USA. [4]Department of Biomedical Sciences, UNC-Lineberger Comprehensive Cancer Center, University of North Carolina, Chapel Hill, North Carolina, USA. [5]Vanderbilt Ingram Cancer Center, Nashville, Tennessee, USA.

Breast cancers that occur in women 2–5 years postpartum are more frequently diagnosed at metastatic stages and correlate with poorer outcomes compared with breast cancers diagnosed in young, premenopausal women. The molecular mechanisms underlying the malignant severity associated with postpartum breast cancers (ppBCs) are unclear but relate to stromal wound-healing events during postpartum involution, a dynamic process characterized by widespread cell death in milk-producing mammary epithelial cells (MECs). Using both spontaneous and allografted mammary tumors in fully immune–competent mice, we discovered that postpartum involution increases mammary tumor metastasis. Cell death was widespread, not only occurring in MECs but also in tumor epithelium. Dying tumor cells were cleared through receptor tyrosine kinase MerTK–dependent efferocytosis, which robustly induced the transcription of genes encoding wound-healing cytokines, including IL-4, IL-10, IL-13, and TGF-β. Animals lacking MerTK and animals treated with a MerTK inhibitor exhibited impaired efferocytosis in postpartum tumors, a reduction of M2-like macrophages but no change in total macrophage levels, decreased TGF-β expression, and a reduction of postpartum tumor metastasis that was similar to the metastasis frequencies observed in nulliparous mice. Moreover, TGF-β blockade reduced postpartum tumor metastasis. These data suggest that widespread cell death during postpartum involution triggers efferocytosis-induced wound-healing cytokines in the tumor microenvironment that promote metastatic tumor progression.

Introduction

Although pregnancy at a young age decreases a woman's lifetime breast cancer risk (1, 2), the first 5 years following a pregnancy at any age are associated with increased breast cancer risk, a risk that continues to increase with age (3–6). Given the societal trends in Western cultures of postponing childbirth later into women's lives, the incidence of malignant postpartum breast cancer is expected to increase. Currently, breast cancers diagnosed 2–5 years postpartum account for nearly 25% of all premenopausal breast cancers (7). Importantly, breast cancers diagnosed 2–5 years postpartum are diagnosed more frequently as metastatic disease and correlate with decreased disease-free survival (DFS) versus breast cancers occurring in premenopausal nulliparous women (4, 7, 8). In contrast, many studies have shown that breast cancers diagnosed during pregnancy do not correlate with decreased DFS (8, 9), although there remains some debate about this conclusion. The observation that postpartum breast cancers (ppBCs) correlate with reduced DFS suggests that events occurring in the postpartum breast augment the malignant severity of tumors existing therein. This hypothesis is supported by studies in which breast cancer cells transplanted into involuting mouse mammary fat pads grow and invade more rapidly than do cells transplanted into mammary glands of nulliparous mice (10–12). This postpartum transplantation model elegantly distinguished the microenvironmental influences of the involuting postpartum mammary gland versus the mammary gland at other reproductive stages (3, 10–15). Thus, it is imperative to understand how the changing landscape of the postpartum breast accelerates cancer progression in order to design more effective therapies for patients suffering from ppBC or strategies to limit the alterations leading to ppBCs.

M2-like macrophages are a critical driving force of malignancy in the postpartum mammary microenvironment through enhanced cyclooxygenase 2 (COX2) production and through enhanced extracellular matrix (ECM) remodeling (16, 17). However, it is unclear what triggers macrophage polarization during postpartum involution toward an M2-like phenotype. Further, cytokines produced by M2-like macrophages (e.g., IL-4, IL-10, IL-13, TGF-β1, and EGF) (18–21) are associated with increased breast cancer malignancy (22–25). It should be noted that these cytokines, which are involved in wound healing and immune suppression, are produced abundantly during postpartum involution to support mammary remodeling (26–29), consistent with their potential involvement in ppBC progression. In addition, our

Note regarding evaluation of this manuscript: Manuscripts authored by scientists associated with Duke University, The University of North Carolina at Chapel Hill, Duke-NUS, and the Sanford-Burnham Medical Research Institute are handled not by members of the editorial board but rather by the science editors, who consult with selected external editors and reviewers.

Conflict of interest: The authors have declared that no conflict of interest exists.

Submitted: March 31, 2014; **Accepted:** August 13, 2014.

Reference information: *J Clin Invest*. 2014;124(11):4737–4752. doi:10.1172/JCI76375.

previous work shows that MerTK, an RTK required for efficient efferocytosis by macrophages and epithelial cells, is elevated during postpartum involution (30) and is involved in the accumulation of Th2-like tumor-associated leukocytes in preclinical mammary tumor models (31).

We have used the *MMTV PyVmT* transgenic mouse model (32) to assess how postpartum mammary involution and remodeling affects malignant progression of spontaneous mammary tumors within the context of their native microenvironment and within a fully competent immune system. Tumor metastasis was elevated 10-fold by events occurring during postpartum involution, triggered by stromal responses to widespread tumor cell death, including increased M2-like macrophage characteristics and enhanced production of wound-healing and immunosuppressive cytokines. These changes in the stromal microenvironment were orchestrated by MerTK, which is responsible in large part for the clearance of dying cells (efferocytosis) by macrophages or other efferocytes. We demonstrate that MerTK inhibition or gene targeting abolished efferocytosis, M2-like macrophage polarization, production of wound-healing cytokines, and reduced tumor metastasis in the postpartum setting. Our data reveal a critical role for MerTK and efferocytosis in driving stromal wound-healing and remodeling events that contribute to ppBC malignancy.

Results

Increased metastasis of tumors in the postpartum mammary gland. Previous studies demonstrated that breast tumor cell lines transplanted into mouse mammary glands just prior to postpartum involution are more invasive and metastatic than the same tumor cells transplanted into the mammary fat pads of age-matched virgin mice (11, 12). We recapitulated these findings using primary mammary tumor cells (PMTCs) derived from *MMTV PyVmT* mice, which we transplanted into the mammary fat pads of WT FVB female mice. Prior to tumor cell injection, age-matched mice (42 days of age) were randomized into 2 groups: 1 remaining nulliparous and 1 that would breed for 1 to 3 days. Primary tumor cells were injected when mice were 59–61 days of age, corresponding to 14.5 to 16.5 dpc in the parous group (Figure 1A), such that partuition occurred 4–7 days after tumor injection. Pups were withdrawn from dams at partuition to initiate postpartum involution in the parous group. Tumors became palpable 11 days (on average) after tumor cell injection in both groups, corresponding to involution day 6 (Inv d6) in the parous group and suggesting that late pregnancy and postpartum events did not affect tumor latency (T_{50} = 11 days, $P > 0.05$, log-rank test). Tumors in parous mice grew at a modestly increased rate compared with what was observed in virgin mice (Figure 1B). However, lungs harvested at postinjection day 39 revealed that metastatic lung lesions occurred in 5 of 6 parous mice, but were not detected in age-matched virgin mice (0 of 6 mice, Supplemental Figure 1; supplemental material available online with this article; doi:10.1172/JCI76375DS1).

We extended these findings using spontaneous tumors arising in *MMTV PyVmT* transgenic mice, with the added advantages of endogenously forming tumors within a fully intact immune system (32). Female mice remained as virgin mice or were impregnated at 42 to 44 days of age. Synchronized pregnancies within this 3-day window allowed us to make age-matched comparisons between genetically comparable animals, establishing reproductive history as the major experimental variable (Figure 1C). In the parous group, pups were withdrawn at partuition because *MMTV PyVmT* dams are unable to nurse their offspring. Pregnancy did not affect average tumor latency (T_{50} = 56 ± 5 days in virgin mice; T_{50} = 52 ± 3 days in parous mice) (Supplemental Figure 2, left panel), total tumor burden (Supplemental Figure 2, right panel), tumor cell proliferation (Supplemental Figure 3), or PyVmT expression (Figure 1D). Histological differences were apparent between virgin and parous groups, including milk within the ductal lumens of parous mouse tumors (but not virgin mouse tumors) at partuition/64 days of age, which was resorbed during the course of postpartum involution (Supplemental Figure 4). Although the number of lung metastases was similar in 64-day-old virgin and parous mice (partuition in the parous group) and in 71-day-old virgin and parous mice (Inv d7 in the parous group), lung metastases in the parous group increased by 10-fold in 85-day-old parous mice (Inv d21) as compared with the metastases seen in 85-day-old virgin mice (Figure 1, E and F). These models demonstrate that changes occurring in the mammary microenvironment during involution have a profound impact on metastasis, without affecting primary tumor burden.

We investigated phosphorylation of STAT3 (p-STAT3) in tumors from virgin and parous mice, as p-STAT3 is an early event in the involution signaling cascade and is known to correlate with increased aggressiveness in several tumor models. We found relatively equal levels of p-STAT3 in parous and virgin mice at 71 days of age (corresponding to Inv d7 in the parous group) and at 85 days of age (corresponding to Inv d21 in the parous group, Figure 1D). We also measured p-AKT and p-ERK, which revealed similar levels of each in virgin and parous mice at 71 days of age (Inv d7 in parous group). At 84 days of age, AKT and ERK phosphorylation was modestly decreased in the parous group (Inv d21) as compared with that detected in the virgin group.

Increased cell death and efferocytosis in postpartum mammary tumors. To begin understanding how postpartum involution might establish a prometastatic tumor microenvironment (TME), we examined the physiological events that characterize postpartum involution in the normal breast. A remarkable feature of postpartum involution is transient but widespread cell death throughout the milk-producing mammary epithelium (33). However, it is currently unknown whether tumors within the breast during postpartum involution are similarly subjected to a vast presence of dying cells. Using TUNEL analysis to measure dying/dead tumor cells, we found very few $TUNEL^+$ cells in tumors from virgin mice at 64 days, 71 days, 85 days, and 104 days of age (Figure 2, A and B). However, the frequency of $TUNEL^+$ cells increased more than 5-fold in tumors harvested from 71-day-old parous mice (Inv d7) and diminished at later involution time points. This is the first demonstration to our knowledge that mammary tumors also experience a peak in cell death during postpartum involution.

During physiological postpartum involution, dying mammary epithelial cells (MECs) are cleared from the mammary gland through efferocytosis, a process by which macrophages and other phagocytes recognize, bind to, and engulf dying cells (34, 35). Macrophages require the RTK MerTK to engulf dying cells, particularly during postpartum involution, when dying cells are

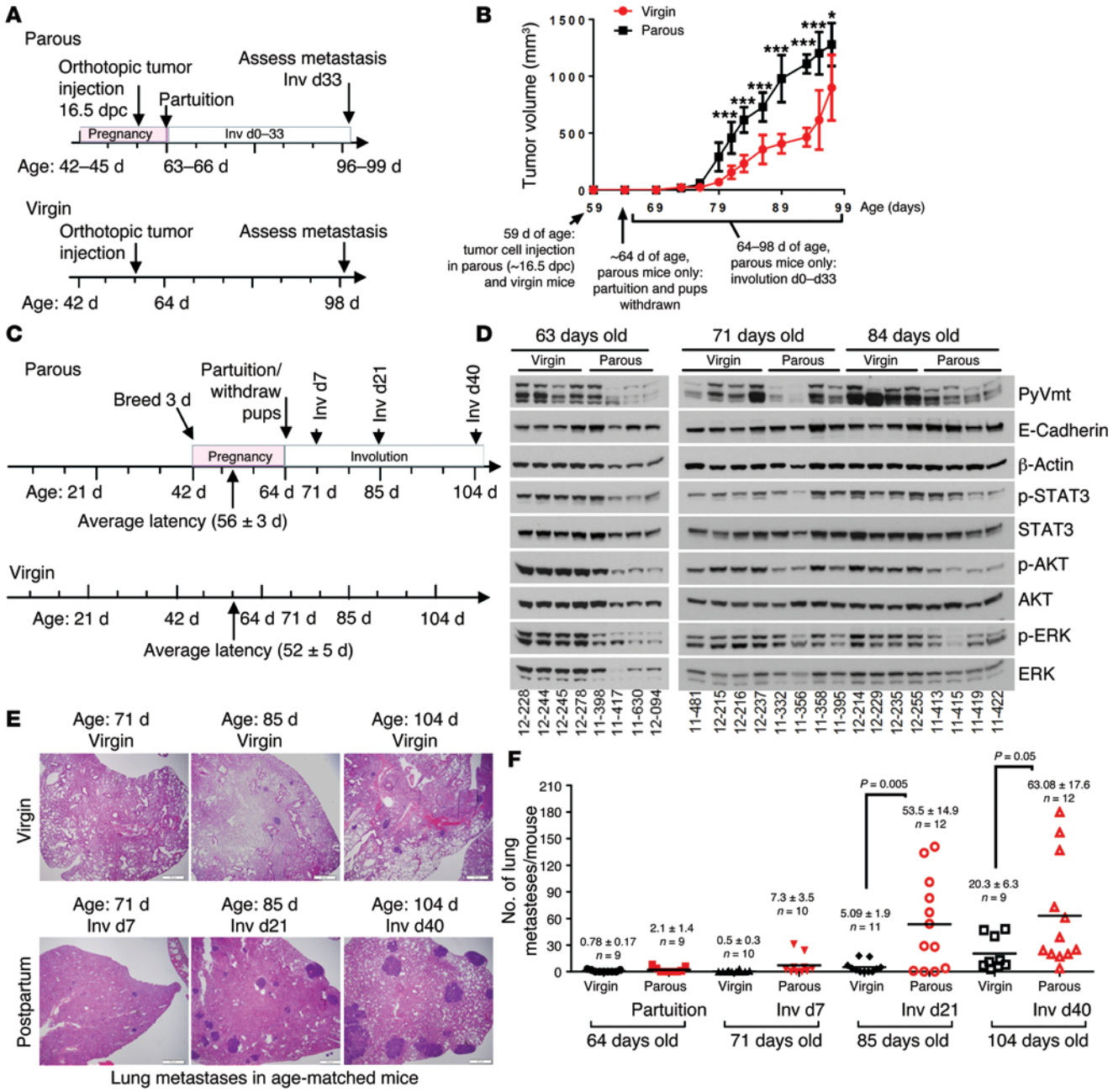

Figure 1. Postpartum involution increases metastasis of mammary tumors. (**A** and **B**) Orthotopic allograft model of ppBC. (**A**) Approach used to model ppBCs in WT female virgin mice. 42-day-old mice were randomized into 2 groups: (a) one that remained nulliparous and (b) one bred for 3 days with WT male mice. Tumors in 56- to 59-day-old mice (14.5–16.5 dpc) were injected. Pups were withdrawn at partuition. Tumors and lungs were harvested from 97-day-old mice (Inv d33 in the parous group). (**B**) Tumor volume, measured 2–3 times per week, is shown as the average tumor volume ± SD. n = 6–8 per group. ; $^*P < 0.05$; $^{***}P < 0.001$. (**C**–**F**) Immune-competent, spontaneous ppBC model. (**C**) Approach used to model ppBCs in *MMTV PyVmT* mice. Female mice were randomized at 42 days of age into 2 groups: (a) one that remained nulliparous and (b) one bred for 3 days with WT male mice. P = NS by log-rank test. (**D**) Whole-tumor lysates assessed by Western blot analysis using the indicated antibodies. Each lane represents tumor lysates harvested from a distinct mouse. (**E**) Representative images of histological lung sections. Original magnification, ×400. (**F**) Quantification of the number of lung metastases per mouse; each point represents a single mouse. Midline represents the average. n = 9–12 per group. P values were calculated by Student's t test.

very abundant (30). In normal mammary glands, MerTK expression is low during puberty, maturity, and pregnancy, but is rapidly induced during postpartum involution, when cell death peaks (30). To determine whether MerTK is similarly induced in postpartum mammary tumors during involution, we used Western blot analysis of whole-tumor lysates collected at partuition (Inv d0) and at postpartum involution time points (Inv d7, Inv d21, and Inv d40). We found that tumor MerTK expression was low at the end of pregnancy (Inv d0, 64 days of age), but was strongly elevated in tumors harvested at Inv d7 (Figure 2C), a time point when TUNEL$^+$ dead tumor cells were at their peak (Figure 2B). Tumor lysates harvested from age-matched *MerTK*$^{-/-}$ mice did not show

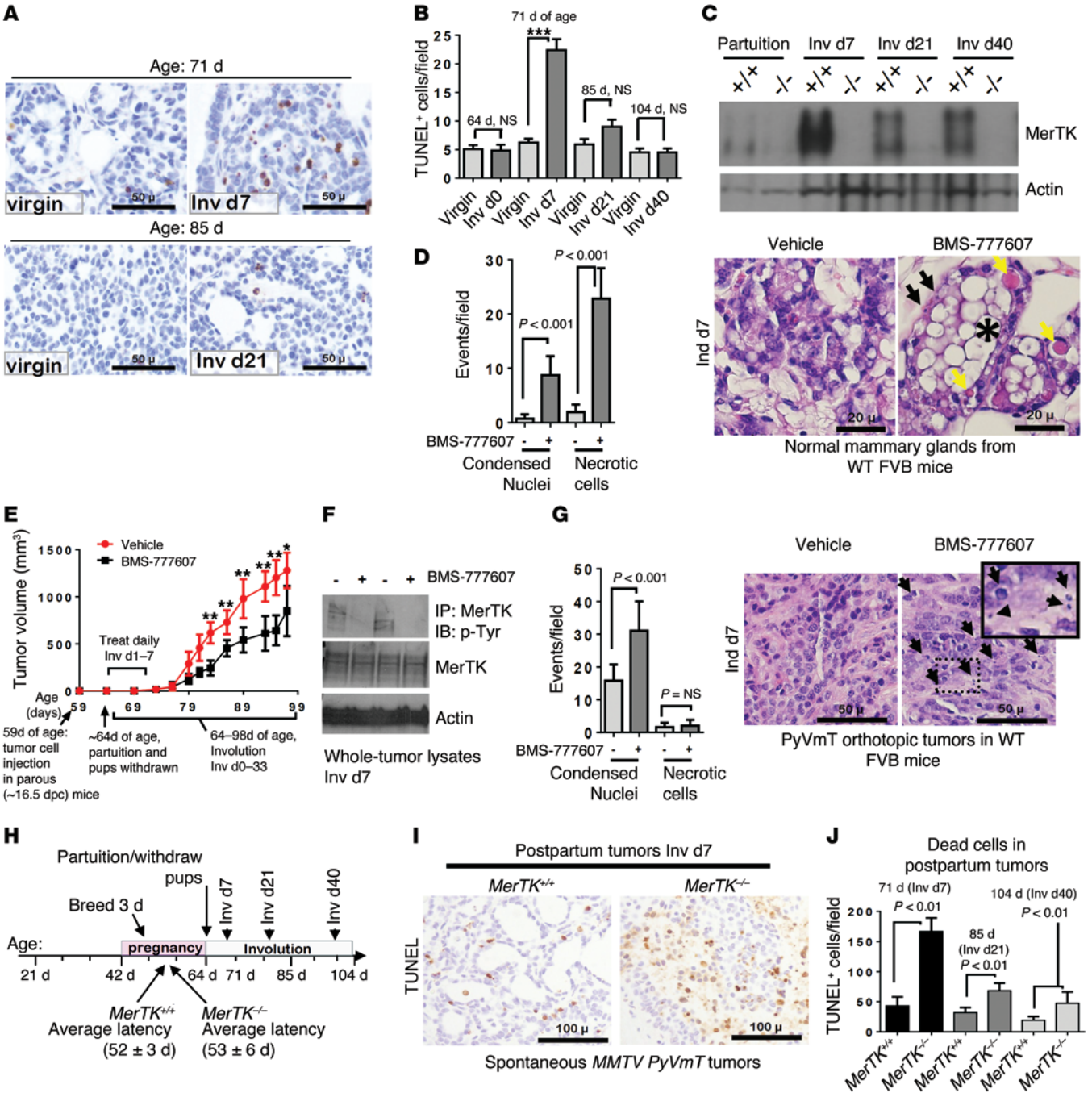

Figure 2. Increased tumor cell death and efferocytosis in ppBCs. (**A**) TUNEL analysis of tumors from virgin and postpartum mice. Representative images are shown. Original magnification, ×400. (**B**) Average TUNEL$^+$ cells per field (5 random fields/sample; n = 4–6). ***$P < 0.001$ by Student's t test. (**C**) Western blot analysis of whole-tumor lysates harvested at partuition (64 days old), Inv d7 (71 days old), Inv d21 (85 days old), and Inv d40 (104 days old). $^{+/+}$ denotes *MerTK*$^{+/+}$ *PyVmT* tumors; $^{-/-}$ denotes *MerTK*$^{-/-}$ *PyVmT* tumors. (**D**) WT mice treated with BMS-777607 (Inv d1–7). Representative histological sections of mammary glands harvested 1 hour after final treatment. Black arrows indicate hypercondensed nuclei of dead cells; yellow areas indicate necrotic cells; single asterisk indicates milk fat globule. Original magnification, ×400. (**E**–**G**) Allografted ppBCs treated with BMS-777607 (Inv d1–7). (**E**) Tumor volume was measured 2–3 times per week and is shown as the average tumor volume ± SD. n = 6–8 per group. **$P < 0.01$; *$P < 0.05$. (**F**) Whole-tumor lysates and MerTK immunoprecipitates from tumor lysates were assessed by Western blot analysis. (**G**) Representative histological sections of tumors harvested 1 hour after final treatment on Inv d7. Arrows indicate hypercondensed nuclei of dead cells. Original magnification, ×400; ×600 (inset). (**H**) Schematic approach to assess ppBCs in *MerTK*$^{+/+}$ *PyVmT* and *MerTK*$^{-/-}$ *PyVmT* mice. Average latency is indicated on timeline. P = NS by log-rank test. (**I**) TUNEL analysis of tumors at Inv d7. Representative images are shown. Original magnification, ×400. (**J**) Average TUNEL$^+$ cells per field (5 fields/sample; n = 4–6 per condition). $P < 0.01$ by Student's t test.

any MerTK expression, as expected. In *MerTK*$^{+/+}$ tumors, postpartum tumor MerTK levels remained elevated throughout Inv d40, as compared with what was detected in tumors harvested at Inv d0, consistent with the hypothesis that MerTK plays an important role in directing efferocytosis in postpartum mammary tumors.

To test this hypothesis directly, we used the MerTK tyrosine kinase inhibitor (TKI) BMS-777607 (36) to impair MerTK activity in mammary tumors during postpartum involution. We first confirmed that BMS-777607 impaired efferocytosis during postpartum involution in normal mammary glands. Beginning at Inv d1, mice were treated with BMS-777607 once daily through Inv d7. MerTK inhibition produced a substantial accumulation of dying/dead cell bodies, necrotic cells, and lipid (milk fat) globules in postpartum mammary glands (Figure 2D), similar to what has been reported in MerTK-deficient mammary glands during postpartum involution (30) and thus confirming that BMS-777607 inhibits MerTK-dependent efferocytosis. Next, we modified the allografted ppBC model shown in Figure 1A, adding daily treatments with BMS-777607 beginning at Inv d1 and ending on Inv d7 (Figure 2E). This brief treatment window coincided with the peak in dying tumor cell burden (Figure 2B) and with the peak induction of MerTK expression (Figure 2C). BMS-777607 treatment for the first 7 days of involution did not affect tumor latency, but caused a slight decrease in the postpartum tumor growth rate. Western blot analysis of MerTK immunoprecipitates from tumor lysates harvested on Inv d7 showed decreased MerTK tyrosine phosphorylation in BMS-777607–treated samples compared with what was detected in vehicle-treated tumors (Figure 2F). Importantly, dead cell bodies were abundant in BMS-777607–treated tumors on Inv d7, but not in vehicle-treated tumors, demonstrating that MerTK signaling is necessary for efferocytosis in postpartum mammary tumors (Figure 2G).

Because BMS-777607 can inhibit other RTKs related to MerTK, we confirmed our findings using genetic MerTK ablation. *MerTK*$^{-/-}$ mice (inbred to FVB) crossed with *MMTV PyVmT* mice were randomized into virgin or breeding groups in which pregnancies were synchronized in 42-day-old mice, as described in Figure 1D. MerTK loss was confirmed in tumors from virgin mice by Western blot analysis of whole-tumor lysates (Supplemental Figure 5A). MerTK loss in virgin mice did not affect tumor latency, total tumor burden, tumor cell proliferation, or tumor cell death (Supplemental Figure 5, B–E). Tumors from virgin *MerTK*$^{-/-}$ and *MerTK*$^{+/+}$ mice were histologically similar (Supplemental Figure 5F). These data are consistent with reports that MerTK expression is not detected in the tumor epithelial cell population of *MMTV PyVmT* tumors (31), explaining in part why MerTK loss had no overt effect on tumor latency or growth in nulliparous mice. However, given the profound burden of dying cells that require clearance from the mammary gland (11, 28, 29, 37) and mammary tumors (Figure 2B) during postpartum involution and the known role of MerTK in efferocytosis, it is possible that MerTK loss uniquely affects tumor progression in the context of postpartum involution.

We examined this hypothesis in tumors harvested from parous *MerTK*$^{+/+}$ and *MerTK*$^{-/-}$ mice at the end of pregnancy/Inv d0 (when pups were withdrawn), Inv d7, Inv d21, and Inv d40 (Figure 2H). MerTK loss was confirmed by Western blot analysis at each time point (Figure 2C). We found that MerTK loss did not affect tumor latency in parous mice (Figure 2H; log-rank test). However, TUNEL analysis revealed a dramatic increase in the presence of dead cell bodies in *MerTK*$^{-/-}$ *PyVmT* tumors at Inv d7 (Figure 2I). Dead cell bodies in *MerTK*$^{-/-}$ tumors remained prominent throughout postpartum Inv d40 (Figure 2J). Because we did not observe increased TUNEL staining in mammary tumors from virgin *MerTK*$^{-/-}$ mice (Supplemental Figure 5E) and because previous studies demonstrate that MerTK is poorly expressed in *MMTV PyVmT* tumor cells (31), these data suggest that MerTK loss did not increase tumor cell death per se, but caused an accumulation of dead cell bodies throughout postpartum involution due to a failure in efferocytosis. This is supported by annexin V staining of purified, cultured *MerTK*$^{+/+}$ *PyVmT* and *MerTK*$^{-/-}$ *PyVmT* primary tumor cells, which revealed similar levels of cell death in both groups (Supplemental Figure 5G).

Pharmacological or genetic MerTK ablation decreases postpartum mammary tumor metastasis. To define the potential relationship between (a) widespread postpartum tumor cell death, (b) efferocytosis of dying tumor cells, and (c) postpartum tumor progression, we examined the impact of pharmacological MerTK inhibition on metastasis of postpartum mammary tumors in our allografted model of ppBC (described in Figure 2E), in which tumor-bearing mice were treated daily with BMS-777607 beginning on Inv d1 and ending on Inv d7. Tumor metastases were counted in lungs harvested at Inv d33 (Figure 3A), revealing metastatic lung lesions in 5 of 6 parous mice treated for 7 days with vehicle, but in only 1 of 6 parous mice treated for 7 days with BMS-777607. These data suggest that MerTK inhibition during early postpartum involution decreases mammary tumor metastasis. Metastases were not detected in the lungs of tumor-bearing virgin mice (with or without BMS-777607 treatment) age-matched to the postpartum group.

These findings were confirmed using genetic MerTK ablation in our spontaneous tumor model of ppBC (described in Figure 2H). We found that although genetic MerTK loss in virgin mice did not affect the number of lung metastases (Figure 3B), MerTK loss in parous mice diminished the number of metastatic lung lesions by more than 3-fold and by more than 6-fold at Inv d21 and Inv d40, respectively (Figure 3C). Importantly, MerTK loss did not affect total tumor burden in parous mice at Inv d0, d7, d21, or d40 (Supplemental Figure 6A), although histological changes associated with impaired efferocytosis were apparent in MerTK-deficient postpartum mammary tumors, such as accumulation of dead cells in fluid-filled lumens (Supplemental Figure 6B), which we confirmed by TUNEL analysis (Supplemental Figure 6C). Taken together, these data establish a relationship between MerTK-mediated efferocytosis and the prometastatic environment in postpartum mammary tumors.

Increased expression of wound-healing cytokines in postpartum mammary tumors. Genes including *Il4*, *Il10*, and *Tgfb1* encoding wound-healing and immunosuppressive cytokines are often induced in response to efferocytosis(38–40). Transcriptional induction of wound-healing and immunosuppressive cytokine signatures is a major feature of the normal mouse mammary gland during postpartum involution (26, 28, 37, 41), due at least in part to high levels of efferocytosis occurring in this setting (30). We used a publicly available quantitative reverse transcription-PCR (qRT-PCR) dataset measuring expression of Th2 cytokine genes

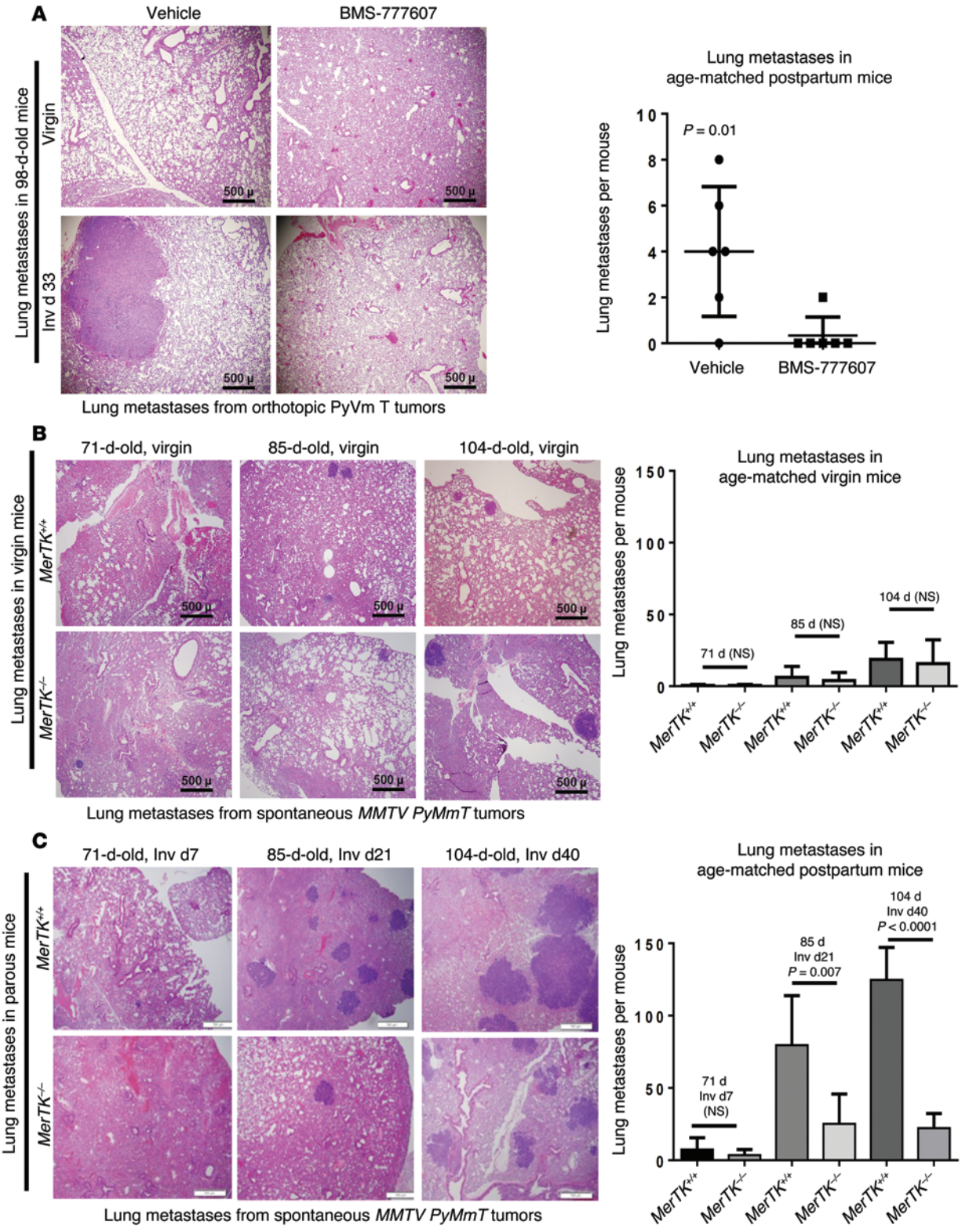

Figure 3. Postpartum involution increases metastasis of ppBCs in a MerTK-dependent manner. (**A**) Left panels: Representative images of histological lung sections harvested from 98-day-old virgin and parous mice harboring orthotopic allografts of mammary tumor cells (corresponding to 38 days after tumor cell injection in both groups and corresponding to Inv d33 in the parous group). Mice were treated with BMS-777607 for 7 days beginning at 64 days of age (corresponding to Inv d1 in the parous group). Right panels: Metastatic burden was quantified from H&E-stained lung sections from all 5 lung lobes in each mouse. $P < 0.01$ by Student's *t* test. Original magnification, ×40. (**B** and **C**) Left panels: Representative histological lung sections from virgin (**B**) and parous (**C**) *MerTK*$^{+/+}$*PyVmT* and *MerTK*$^{-/-}$*PyVmT* mice. Original magnification, ×40. Right panels: Metastatic burden was quantified from H&E-stained lung sections from all 5 lung lobes in each mouse. *P* values were calculated by Student's *t* test.

in human breast tissue specimens collected from premenopausal women who were either nulliparous or who were within 0 to 2 years of a recent full-term pregnancy (27). These data revealed elevated *IL13* and *TGFB1* levels in postpartum samples (n = 4–13) compared with what was seen in samples from nulliparous women (n = 4–20) (Figure 4A). *IL4* was not reported in this dataset, although mouse models have shown upregulation of *Il4* during postpartum involution (16, 26, 42). Levels of *CD68* (a molecular marker for total macrophage content), *IFNG* (a Th1-like cytokine), and *CDH1* (encoding E-cadherin, to control for epithelial content) were similar in samples harvested from nulliparous and postpartum women. These findings suggest that transcripts encoding wound-healing or Th2-like cytokines are locally elevated in postpartum breast tissue in humans, similar to what is seen in mice, supporting the utility of mouse mammary tumor models to understand how postpartum changes in the breast microenvironment contribute to deadly tumor metastasis.

To determine whether postpartum mammary tumors upregulate wound-healing and immune-suppressive cytokines, we compared cytokine levels in spontaneous *MMTV PyVmT* tumors harvested from 71-day-old virgin and parous (Inv d7) mice. Using a cytokine antibody array to gain a broad and unbiased view of cytokine expression in postpartum mammary tumors (Supplemental Figure 7), we found that IL-4 and IL-10 were detected at very low levels in tumors from virgin mice, but were upregulated in tumors from postpartum (Inv d7) mice (Figure 4B). Most cytokines examined were similar in virgin and postpartum tumors (Supplemental Figure 7), including osteopontin (Figure 4B). Cytokine transcripts measured by qRT-PCR analysis of whole-tumor RNA harvested confirmed *Il10*, *Il4*, and *Tgfb1* upregulation in postpartum mammary tumors over what was seen in tumors from virgin mice (Figure 4C), demonstrating that these wound-healing cytokines are locally synthesized in the postpartum mammary TME. It should be noted that wound-healing Th2-like cytokines are frequently detected in clinical breast tumors (24, 43) and are associated with decreased DFS in breast cancer patients (24, 43).

Decreased wound-healing cytokines in postpartum MerTK$^{-/-}$ tumors. Macrophage-mediated efferocytosis is known to trigger the production of wound-healing Th2-like cytokines, including IL-10 and TGF-β1, although the link between tumor cell efferocytosis and TME cytokine levels has not been widely investigated. If efferocytosis in postpartum breast tumors is the primary trigger for the production of Th2-like cytokines, we predicted that the blockade of efferocytosis through MerTK inhibition would prevent postpartum induction of wound-healing cytokines in tumors. We tested this hypothesis using a cytokine antibody array of whole-tumor lysates from postpartum *MerTK*$^{+/+}$ and *MerTK*$^{-/-}$ mammary tumors harvested at Inv d7 (Figure 4D). Postpartum *MerTK*$^{-/-}$ tumors exhibited decreased IL-4, IL-10, and IL-13 levels as compared with the levels detected in *MerTK*$^{+/+}$ tumors (Figure 4E). Most of the cytokines we examined were measured at similar levels in postpartum *MerTK*$^{+/+}$ and *MerTK*$^{-/-}$ tumors (Supplemental Figure 8). These results were confirmed by qRT-PCR analysis of whole-tumor RNA, revealing reduced *Il4*, *Il10*, and *Tgfb1* transcripts in postpartum *MerTK*$^{-/-}$ mammary tumors as compared with those detected in postpartum *MerTK*$^{+/+}$ tumors (Figure 4F). Similarly, whole-tumor RNA from allografted tumors treated with BMS-777607 from Inv d1 to Inv d7 revealed decreased *Il10* and *Tgfb1* mRNAs, although *Il4* transcripts were not altered by BMS-777607 (Figure 4G). These studies suggest that MerTK-mediated efferocytosis enhances wound-healing Th2-like cytokine levels in postpartum mammary tumors.

Efferocytosis of dying breast cancer cells induces Th2-like cytokine expression. To investigate a mechanistic link between postpartum tumor cell death and cytokine modulation by tumor-associated macrophages, we generated a coculture-based model in which dying breast cancer cells could be engulfed by neighboring macrophages. To generate a model of dying mammary tumor cells, we transduced PyVmT primary mammary tumor cells expressing fluorescent mCherry with adenovirus expressing herpes simplex virus-thymidine kinase (HSV-TK), rendering these cells sensitive to gancyclovir-inducible cell death (Figure 5A). After 32 hours in the presence of gancyclovir, *PyVmT mCherry TK* cells displayed more than 85% cell death (Figure 5B and Supplemental Figure 9). These *PyVmT mCherry TK* cells were cocultured with GFP-labeled mouse macrophages (Raw267.4), followed by treatment of cocultures with gancyclovir to induce cell death specifically in the tumor cell population (but not in neighboring macrophages) (Figure 5B and Supplemental Figure 9). BMS-777607 was used in this coculture model to block MerTK activity. Cocultures treated with BMS-777607 (1 μM) displayed reduced MerTK tyrosine phosphorylation (Figure 5C), as did cocultures treated with a goat anti-mouse MerTK-neutralizing antibody (ref. 44 and Supplemental Figure 10).

Fluorescence microscopy demonstrated that many dying *PyVmT mCherry TK* tumor cells were contained within cytoplasmic vacuoles of GFP$^+$ macrophages (Figure 5D, white arrows), while others remained free in culture (Figure 5D, yellow arrows). However, cocultures treated with BMS-777607 failed to exhibit any mCherry$^+$ inclusions within GFP$^+$ macrophages, confirming that efferocytosis was blocked by BMS-777607. *PyVmT mCherry TK* cells remaining in culture after 32 hours were counted, revealing a loss of 68.7% of gancyclovir-treated *PyVmT mCherry TK* tumor cells after 32 hours in coculture with macrophages, as compared with the number of recovered *PyVmT mCherry TK* tumor cells lacking gancyclovir treatment or lacking macrophage coculture (Figure 5E). Importantly, BMS-777607 blocked the clearance of dying *PyVmT mCherry TK* tumor cells. We obtained similar findings using *MCF7 mCherry* human breast cancer cells infected with Ad.TK (Supplemental Figure 9), which revealed reduced recovery of dying *MCF7 mCherry TK* cells in the presence of macrophages. BMS-777607 inhibited clearance of dying *MCF7 mCherry TK* tumor cells by Raw264.7 macrophages (Figure 5F). Similarly, preincubation of cocultures with a neutralizing anti-mouse MerTK antibody prior to treatment with gancyclovir impaired the clearance of dying *MCF7 mCherry TK* tumor cells, confirming the role of MerTK in this macrophage-mediated process (Figure 5F).

To investigate efferocytosis-induced changes in cytokines, the efferocytosis coculture assay required modification because Ad.TK altered cytokine levels, even in the absence of efferocytosis (not shown). Therefore, we induced cell death in nonadherent suspensions of MCF7 cells using the Bcl-2/Bcl-xL inhibitor ABT-263 (1 μM) in combination with the phosphatidylinositol-3 kinase (PI3K) inhibitor BKM-120 (1 μM) for 4 hours (Figure 5G). Cells were washed 5 times to remove residual drug, then were cultured

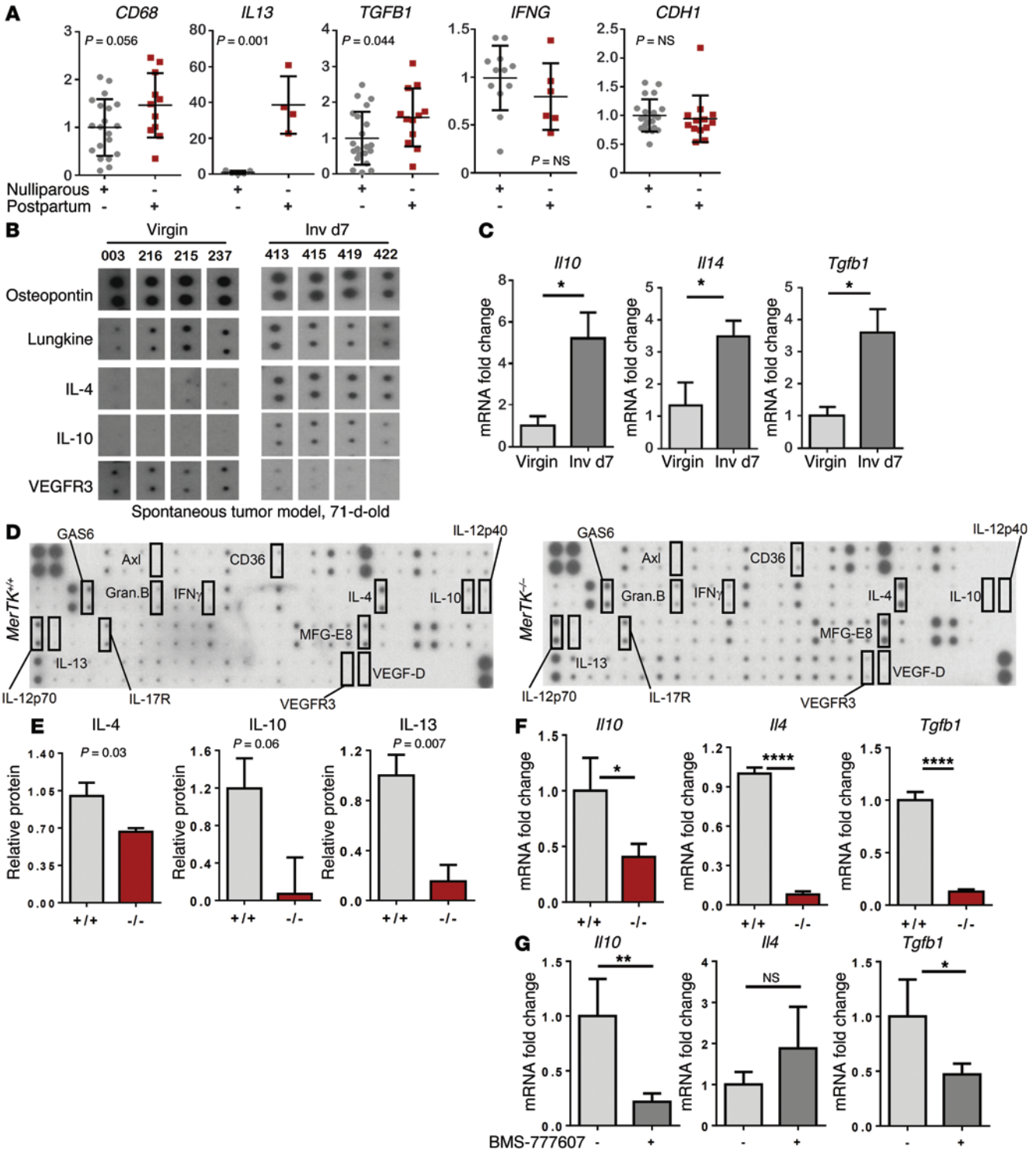

Figure 4. Increased expression of Th2-like cytokines in postpartum tumors requires MerTK. (**A**) A publicly available qRT-PCR dataset of RNA expression levels in normal breast biopsies harvested from premenopausal nulliparous women and premenopausal women 0–2 years after a full-term pregnancy (27) was queried for relative expression levels of the indicated transcripts, which were normalized to dataset housekeeping genes. *P* values were calculated by Student's *t* test. *n* = 4–20 per group. (**B**) Cytokine antibody array was performed using lysates from spontaneous *MMTV PyVmT* tumors harvested from 71-day-old mice (*n* = 4 tumors per group). Individual cytokine spots are shown from identical exposures. (**C**) Whole-tumor RNA from 71-day-old virgin and postpartum (Inv d7) mice was assessed by qRT-PCR for *Il10*, *Il4*, and *Tgfb1*. Values are the average relative transcripts levels ± SD. *n* = 4 tumors analyzed in 6 replicate experiments. **P* < 0.05 by Student's *t* test. (**D**) Cytokine antibody array was performed using lysates from *MerTK*$^{+/+}$ *PyVmT* and *MerTK*$^{-/-}$ *PyVmT* postpartum tumors (Inv d7). *n* = 4. (**E**) Densitometry-based quantitation of relative cytokine levels in whole-tumor lysates. Selected cytokines of interest are shown. Values are the average ± SD. *n* = 4. *P* values were calculated by Student's *t* test. (**F**) RNA isolated from whole tumors collected from 71-day-old parous *MerTK*$^{+/+}$ *PyVmT* and *MerTK*$^{-/-}$ *PyVmT* mice at Inv d7 was assessed by qRT-PCR to quantify *Il10*, *Il4*, and *Tgfb1*. Values shown are the average ± SD. *n* = 4. **P* < 0.05; *****P* < 0.0001 by Student's *t* test. (**G**) RNA isolated from whole tumors from parous mice treated from Inv d0 to Inv d7 with or without BMS-777607 was assessed by qRT-PCR to quantify *Il10*, *Il4*, and *Tgfb1*. Values shown are the average ± SD. *n* = 4. **P* < 0.05; ***P* < 0.01 by Student's *t* test.

alone or in combination with Raw267.4 mouse macrophages. Annexin V staining revealed that this approach induced cell death in more than 70% of all MCF7 cells (Supplemental Figure 11). After 16 hours of coculture, we used ELISAs to measure protein levels of mouse IL-4 (mIL-4) and mIL-10 in the cultured media. The use of mouse macrophages to engulf human breast cancer cells allowed us to exploit antibody specificity to capture mouse cytokines (macrophage-derived, in this case), while excluding human cytokines (tumor cell–derived, in this case). When macrophages, dying MCF7 cells, or live MCF7 cells were cultured alone in serum-free media, only low levels of mIL-4 and mIL-10 were detected (Figure 5H). However, coculture of macrophages with dying MCF7 cells, but not live MCF7 cells, significantly increased mIL-4 and mIL-10 (Figure 5H). Whole-cell RNA after 16 hours revealed increased *Tgfb1* transcript levels in macrophages cocultured with dying MCF7 cells, but not with live MCF7 cells (Figure 5H). Further, MerTK inhibition using BMS-777607 or goat anti-mouse MerTK-neutralizing antibody decreased mIL-4 levels in cultured media (Figure 5I). We found that induction of mIL-10 occurred when macrophages were cocultured with dead MCF7 cells, but not in the presence of the neutralizing MerTK antibody (Supplemental Figure 12). These data suggest that MerTK-dependent efferocytosis of dying breast cancer cells induces Th2-like cytokines in the postpartum TME.

Increased infiltration of tumor-associated macrophages in postpartum mammary tumors. During physiological postpartum involution, macrophages expressing M2-like (alternatively activated) molecular markers, such as arginase 1 (ARG1) or CD206, are the predominant macrophage population in the mammary gland (16, 45, 46). Importantly, M2 macrophages increase the malignancy of ppBCs in transplantable models (10, 13). We examined the impact of postpartum involution on macrophages in spontaneous *MMTV PyVmT* tumors (Figure 6A). Immunofluorescence detection of the macrophage marker F4/80 revealed that macrophage density was similar in tumors from 71-day-old virgin and postpartum mice (Inv d7) (Figure 6B). However, macrophages localized to the tumor periphery in samples from virgin mice, but infiltrated the tumor epithelium of postpartum tumors, in agreement with what is known regarding macrophages in postpartum involution (16). We measured ARG1 by IHC in mammary tumors from virgin or postpartum (Inv d7) mice (Figure 6C), finding substantially increased ARG1 in tumors harvested during postpartum involution compared with what was found in virgin samples (Figure 6D). Expression of *Mrc1*, the gene encoding the M2 molecular marker CD206, was also markedly elevated in whole-tumor RNA harvested at Inv d7 (Figure 6E). These findings were confirmed in samples harvested from allografted PyVmT tumors, revealing that *Mrc1* levels were also higher in tumors harvested at postpartum Inv d7 compared with what we observed in tumors from age-matched virgin mice (Figure 6E). In contrast, *Nos2* (encoding iNOS, a marker of M1-like macrophages) was expressed at similar levels in tumors from 71-day-old virgin and 71-day-old postpartum mice (Supplemental Figure 13). Thus, postpartum involution increases intratumoral M2-like macrophages, consistent with what has been reported for the normal mammary gland during involution and in other models of ppBC.

To determine whether MerTK-mediated efferocytosis is a critical driving force for M2 macrophage polarization in postpartum mammary tumors, we assessed macrophages in spontaneous *MMTV PyVmT* mammary tumors from parous $MerTK^{+/+}$ and $MerTK^{-/-}$ mice at postpartum Inv d7 (Figure 6F). Loss of MerTK did not affect total macrophage density and did not affect the number of intratumoral macrophages (Figure 6G), suggesting that MerTK and efferocytosis are not required to recruit tumor macrophages during postpartum involution. However, postpartum $MerTK^{-/-}$ tumors harvested at Inv d7 harbored fewer $ARG1^{+}$ cells (the M2-like marker) (Figure 6, H and I) and expressed decreased *Mrc1* levels as compared with postpartum $MerTK^{+/+}$ mammary tumors (Figure 6J). Additionally, pharmacological inhibition of MerTK using BMS-777607 from Inv d1 to Inv d7 resulted in decreased *Mrc1* expression levels (Figure 6J). These data suggest that MerTK signaling in the TME during postpartum involution does not affect macrophage recruitment to tumors, but enhances the acquisition or maintenance of M2-like phenotypes of macrophages in postpartum tumors. Importantly, these data indicate that MerTK inhibition can be used to diminish M2-like macrophage phenotypes in postpartum mammary tumors.

Increased TGF-β signaling increases mammary tumor metastasis during postpartum involution. To determine the impact of efferocytosis-induced cytokines on postpartum mammary tumor metastasis, we used an antibody-based approach to neutralize 2 candidate cytokines, IL-4 and TGF-β1, in postpartum tumors (Figure 7A). Beginning at partuition, tumor-bearing WT mice were treated with the mIL-4 antibody 11B11 twice weekly through Inv d14. Western blot analysis of whole-tumor lysates confirmed immune depletion of IL-4 from postpartum tumors (Figure 7B). Despite decreased IL-4 in the TME, the number of metastatic lung lesions was statistically similar in mice treated with 11B11 compared with the number of lesions in mice treated with an isotype-matched IgG (Figure 7C).

In contrast, tumor-bearing mice treated with the anti-mouse TGF-β–neutralizing antibody 1D11 twice weekly through Inv d14 displayed reduced levels of p-Smad2 in whole-tumor lysates at Inv d15 (Figure 7D) and reduced numbers of metastatic lung lesions at Inv d40 (Figure 7E) as compared with tumors treated with isotype-matched IgG. These findings suggest that efferocytosis-induced TGF-β expression increases TGF-β signaling in mammary tumor cells during postpartum involution to enhance tumor metastasis. Interestingly, postpartum tumors treated with the IL-4 antibody 11B11 displayed a further increase in *Tgfb1* mRNA (Supplemental Figure 14A) and increased p-Smad2, a TGF-β–activated transcription factor (Supplemental Figure 14B).

TGF-β signaling is known to increase motility and invasion of mammary tumor cells. To determine whether efferocytosis is capable of inducing TGF-β–mediated tumor cell invasion, we first established efferocytosis cocultures composed of dead MCF7 cells (as established in Figure 5G) cocultured with Raw267.4 macrophages and collected the cultured media after 16 hours (efferocytosis-conditioned media) (Figure 7F). We used media from cocultures of live MCF7 cells with Raw267.4 macrophages for comparison (live cell–cocultured media). We used efferocytosis-conditioned media to stimulate serum-starved recipient PyVmT primary tumor cells in

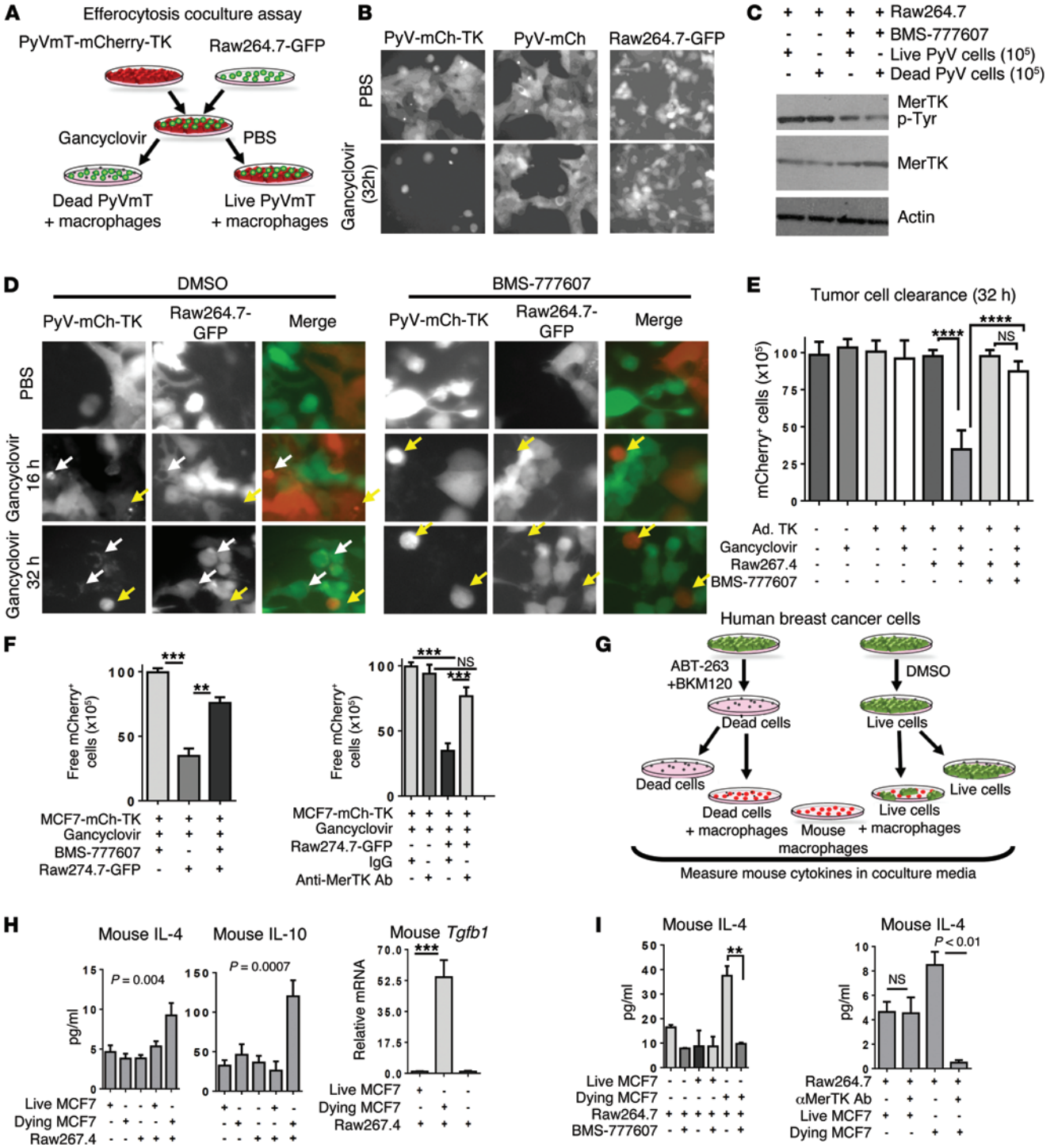

Figure 5. MerTK-dependent efferocytosis of dying breast cancer cells induces production of TGF-β, IL-10, and IL-4. (**A**) Schematic of a novel breast cancer efferocytosis coculture assay. PyVmT cells expressing mCherry and HSV-TK were cocultured with GFP-Raw264.7 macrophages. Gancyclovir caused cell death in HSV-TK$^+$ PyVmT cells. BMS-777607 or neutralizing anti-MerTK antibody was used to block MerTK-dependent efferocytosis. (**B**) Gancyclovir-inducible cell death in PyVmT cells. Original magnification, ×400. (**C**) Western blot analysis of whole-cell lysates or MerTK immunoprecipitates from cocultures treated with or without BMS-777607 (1 μM) for 16 hours. (**D**) Representative fluorescent images of cocultures. White arrows indicate condensed mCherry$^+$ tumor cells within cytoplasmic vacuoles of GFP$^+$ macrophages; yellow arrows indicate condensed mCherry$^+$ cells free in culture. Original magnification, ×400. (**E**) mCherry$^+$ cells remaining after 32 hours in coculture. $^{****}P < 0.0001$ by Student's *t* test. (**F**) Remaining MCF7-mCherry cells were quantified. Values represent the average ± SD. $^{**}P < 0.01$; $^{***}P < 0.001$. $n = 6$. (**G**) MCF7-mCherry cells were cultured for 4 hours in suspension with BKM120 (1 μM) plus ABT-263 (2 μM) to induce cell death, then seeded over adherent Raw264.7 cells and cocultured for 16 hours with or without BMS-777607 or anti-MerTK antibody. (**H**) Mouse IL-4 and IL-10 ELISA of cultured media and qPCR to measure mouse *Tgfb1* transcripts in whole coculture RNA. Values represent the average ± SD. $n = 4$, each assessed in duplicate. $^{**}P < 0.01$. (**I**) Mouse IL-4 ELISA of cocultured media. $n = 4$, each sample assessed in duplicate. Values are the average ± SD. $^{**}P < 0.01$ by Student's *t* test. PyV-mCh-TK, PyVmT-mCherry-TK; PyV-mCh, PyVmT-mCherry.

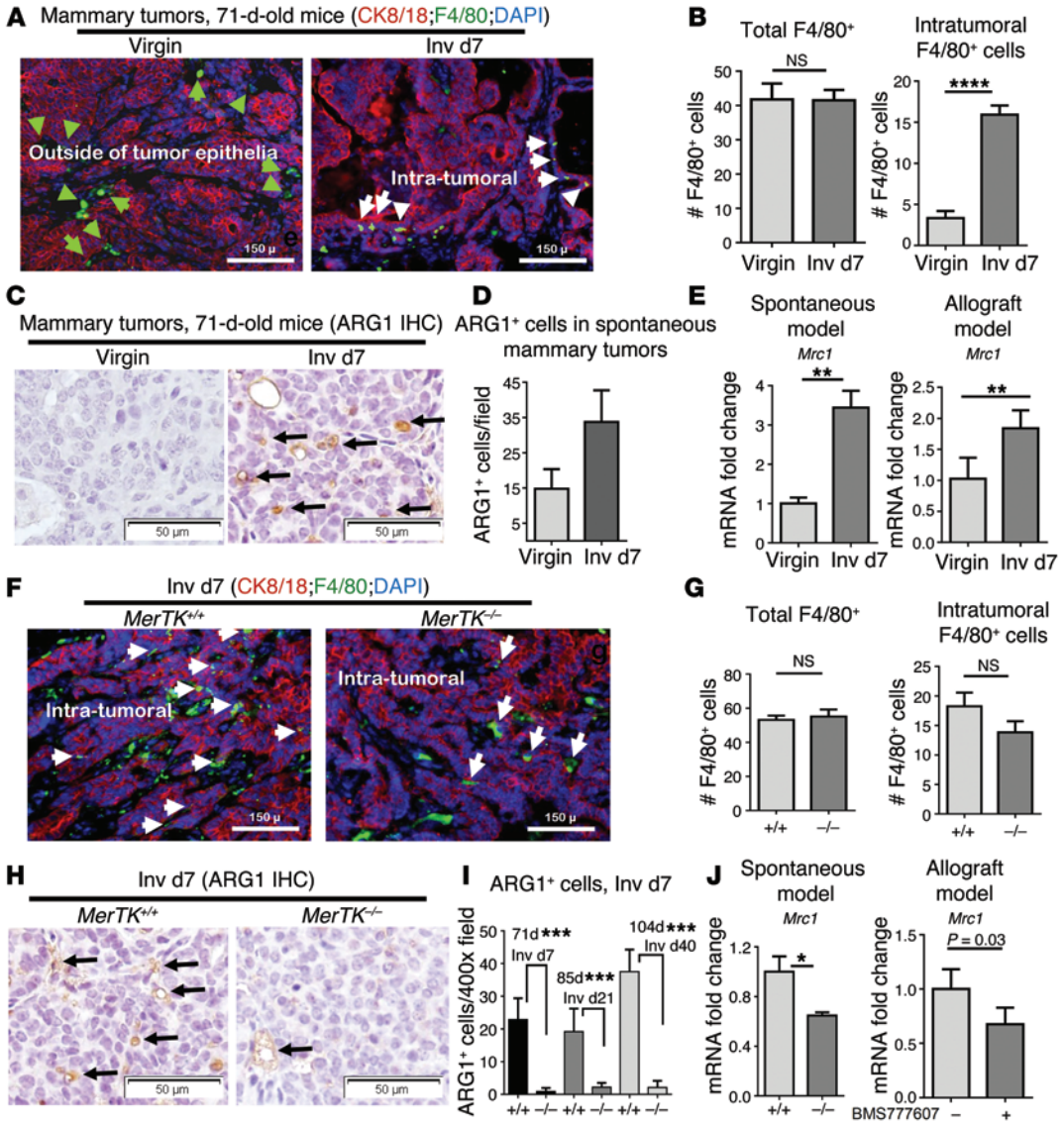

Figure 6. M2 polarization of postpartum tumor–associated macrophages requires MerTK. (**A**–**E**) Tumor sections of *MMTV PyVmT* spontaneous mammary tumors from 71-day-old virgin and postpartum mice were used for analysis. (**A**) Representative immunofluorescent images showing CK8/18 (red) and F4/80 (green) staining; nuclei were counterstained with DAPI (blue). $n = 4$. Green arrows indicate peritumoral F4/80$^+$ macrophages; white arrows indicate intratumoral macrophages. Original magnification, ×100. (**B**) Average (± SD) number of total (left panel) and intratumoral (right panel) macrophages per ×400 field. $n = 4$, 5 fields per sample. $^{****}P < 0.0001$ by Student's t test. (**C**) Representative images of IHC ARG1 staining. $n = 4$. Original magnification, ×400. (**D**) Average number of ARG1$^+$ cells per ×400 field. ($n = 4$). Values are the average ± SD. $P < 0.001$ by Student's t test. (**E**) Whole-tumor RNA assessed by qRT-PCR to quantify relative *Mrc1*. Values shown are the average ± SD. $n = 4$. $^{**}P < 0.01$ by Student's t test. (**F**–**J**) *MerTK*$^{+/+}$ *PyVmT* and *MerTK*$^{-/-}$ *PyVmT* postpartum mammary tumors from 71-day-old mice. (**F**) Representative immunofluorescent images of CK8/18 (red) and F4/80 (green) staining; nuclei were counterstained with DAPI (blue). $n = 4$. White arrows indicate intratumoral macrophages. (**G**) Total (left panel) and intratumoral macrophages (right panel) per ×400 field. $n = 4$, 5 fields per sample. Values are the average ± SD. Student's t test. (**H**) Representative IHC images of ARG1 staining. Original magnification, ×400. (**I**) Average number of ARG1$^+$ cells per ×400 field. $n = 4$. Values are the average ± SD. $^{***}P < 0.001$ by Student's t test. (**J**) Whole-tumor RNA assessed by qRT-PCR to quantify *Mrc1*. Values are the average ± SD. $n = 4$. $^{*}P < 0.05$ by Student's t test.

culture, inducing p-Smad2 to a greater extent than cultured media harvested from "live cell" cocultures (Figure 7G). We found that p-Smad2 induced in response to efferocytosis-conditioned media was inhibited by the TGF-β receptor type 1 (TβR1) inhibitor SD208 (1 μM), confirming that bioavailable TGF-β is upregulated in response to efferocytosis. Efferocytosis-conditioned media increased invasion of PyVmT primary tumor cells through Matrigel-coated Transwell filters (Figure 7H), as did recombinant TGF-β1 (2 pg/ml). Invasion through Transwell filters in response to both efferocytosis-conditioned media and TGF-β1 was blocked by the TβR1 inhibitor SD208.

These results suggest that efferocytosis induces TGF-β in the postpartum mammary TME, thus enhancing tumor cell invasion and migration. This hypothesis was tested in a 3D invasion assay, in which spheroids generated from human breast cancer–derived cell lines (MDA-MB-361 and SKBR3) were embedded in a collagen matrix (2.5 mg/ml), then cultured for 24 hours. Cultures were imaged at 0 and 24 hours following TGF-β1 treatment, revealing that TGF-β1 increased cellular invasion away from spheroids into the surrounding collagen matrix (Figure 7I). We observed that tumor cell invasion from spheroids was inhibited by SD208 (Figure 7J). Similarly, efferocytosis-conditioned media (but not live cell–conditioned media) induced invasion of tumor cells from the spheroid into the collagen matrix, but was blocked upon treatment with SD208. Altogether, these data suggest that increased metastasis of postpartum breast tumors is due in large part to efferocytosis-dependent cytokine modulation in the postpartum mammary gland and identify MerTK and TGF-β as potential therapeutic targets to improve the outcome for young women diagnosed with ppBC (Figure 7K).

Discussion

Premenopausal breast cancers diagnosed during postpartum involution are more frequently diagnosed at metastatic stages as compared with premenopausal breast cancers diagnosed in nulliparous women, pregnant women, or women whose pregnancies occurred more than 10 years before diagnosis (5–8). We have used a spontaneous model of breast cancer to study postpartum mammary tumors within the context of the native TME and a fully competent immune system. Postpartum involution profoundly increased tumor metastasis in this spontaneous tumor model. We verified the results using an allografted mammary tumor model introduced at late pregnancy, which would be less influenced by pregnancy-associated events. Results from the present study establish a causal relationship between the tissue remodeling events of physiological postpartum involution and the increased metastasis of postpartum mammary tumors. Both scenarios are characterized by a transient widespread wave of cell death, efferocytosis, M2 macrophage polarization, and production of key wound-healing cytokines, of which the latter 2 correlate with advanced disease and reduced DFS in breast cancer patients (16, 24, 25, 43).

Our results suggest that increased tumor cell death during postpartum involution triggers efferocytosis, which then induces a stromal wound-healing response that enhances tumor malignancy. Importantly, we identified that MerTK, a critical regulator of efferocytosis in physiological postpartum involution (30), is also required for efferocytosis in postpartum mammary tumors during involution, driving M2 macrophage polarization and wound-healing cytokine production. Pharmacological MerTK inhibition using BMS-777607 reduced efferocytosis, wound-healing cytokines, and metastasis in postpartum mammary tumors. Although BMS-777607 also inhibits Met, Ron, Axl, and Tyro3 (36), we confirmed that MerTK uniquely performs these roles in postpartum mammary tumors using genetic MerTK ablation (Supplemental Figure 15). Additional studies will be required to determine how these other RTKs contribute to postpartum tumor progression, but we propose that BMS-777607 might be used for short durations during postpartum breast remodeling as a potential strategy to inhibit MerTK-mediated efferocytosis and the wound-healing events that follow.

A widespread burden of dying cells in any healthy or injured tissue requires a mechanism to clear dying cells (47–49). In some tissues, such as the epidermis or the gut, dying cells can be sloughed. However, in other tissues, including the retina or the involuting mammary gland, removal of dying cells is achieved through efferocytosis, a process that relies on MerTK (49–52). MerTK recognizes, binds to, and engulfs dying cells marked by phosphatidyl serine (PS), doing so in conjunction with its ligands (Gas6, protein-S, galectin-3, Tubby, and Tubby-like protein 1 [TULP-1]; reviewed in ref. 39]. Efferocytosis is known to produce a shift in macrophage phenotypes toward M2-like characteristics (albeit through unknown mechanisms) and to induce transcription of Th2-like cytokines, including *Il10* and *Tgfb1* (53–55). Genetically engineered mouse models demonstrated that signaling through IL-4 and TGF-β also enhances M2 macrophage polarization (21, 56, 57). Thus, it is possible that MerTK initiates M2 macrophage polarization through efferocytosis-mediated induction of IL-4 and TGF, although this hypothesis remains to be tested. Based on our findings herein, we propose that MerTK-dependent efferocytosis is the driving force behind changes in cytokine levels during physiological postpartum involution and in postpartum mammary tumors. This hypothesis is supported by previous studies showing that MerTK loss from the mammary gland during physiological postpartum involution reduces efferocytosis of dying MECs, causing impaired upregulation of *Il10* and *Tgfb1* (30). Other studies demonstrated that MerTK-mediated efferocytosis of dying neutrophils or injured cardiomyocytes, liver cells, or lung epithelial cells induces the transcription of wound-healing cytokines that promote resolution of acute inflammation and tissue repair (47, 50, 54, 58–62). While MerTK-mediated efferocytosis is desirable in physiological (e.g., postpartum involution of the breast) or pathological (e.g., tissue damage) wound-healing situations, our results suggest that efferocytosis-mediated tissue repair in tumors would enhance tumor metastasis. We show herein that MerTK was in large part responsible for the exaggerated metastasis of ppBCs and for a robust M2-like macrophage presence in postpartum tumors, without affecting total tumor macrophage content. Thus, our studies provide the first illustration to our knowledge of how efferocytosis promotes malignant cancer progression in the endogenous TME.

These findings are consistent with previous reports indicating that loss of MerTK or its ligand Gas6 decreases tumor malignancy in transplantable tumor models in virgin mice, without affecting macrophage recruitment to tumors (31, 63). The previous studies reported that adoptive transfer of MerTK-deficient bone marrow reduced tumor growth over the course of 20 weeks and altered tumor cytokine levels, although lung metastasis and efferocytosis were not reported in this model (31). Together, the current and previous studies suggest that MerTK inhibition reduces tumor malignancy through impaired efferocytosis-induced cytokine modulation. Conversely, increased MerTK expression correlates with decreased DFS in many cancers and may decrease tumor response to chemotherapies (64–66), albeit through unknown mechanisms.

Our results indicate that efferocytosis-induced expression of TGF-β1 increases invasion and motility of mammary tumors cells and that blocking MerTK for the first 7 days of involution, or blocking TGF-β for the first 14 days of involution, is sufficient to impair formation of lung metastases through later time points. The observation that a 7-day time course of MerTK inhibition during early involution was sufficient to provide a therapeutic effect is of great interest, as a potential on-target side effect of sustained MerTK inhibition may be increased autoimmunity. Limited use of a MerTK inhibitor during a short postpartum window would minimize the risk of developing autoimmunity and may be sufficient to limit the profound wound-healing response initiated by efferocytosis during postpartum involution.

In summary, we have shown that changes that occur during physiological postpartum involution, including widespread cell death, MerTK-dependent efferocytosis, and induction of wound-healing cytokines, similarly occur in postpartum mammary tumors, enhancing tumor metastasis. This knowledge will advise new potential strategies for the prevention and treatment of ppBCs.

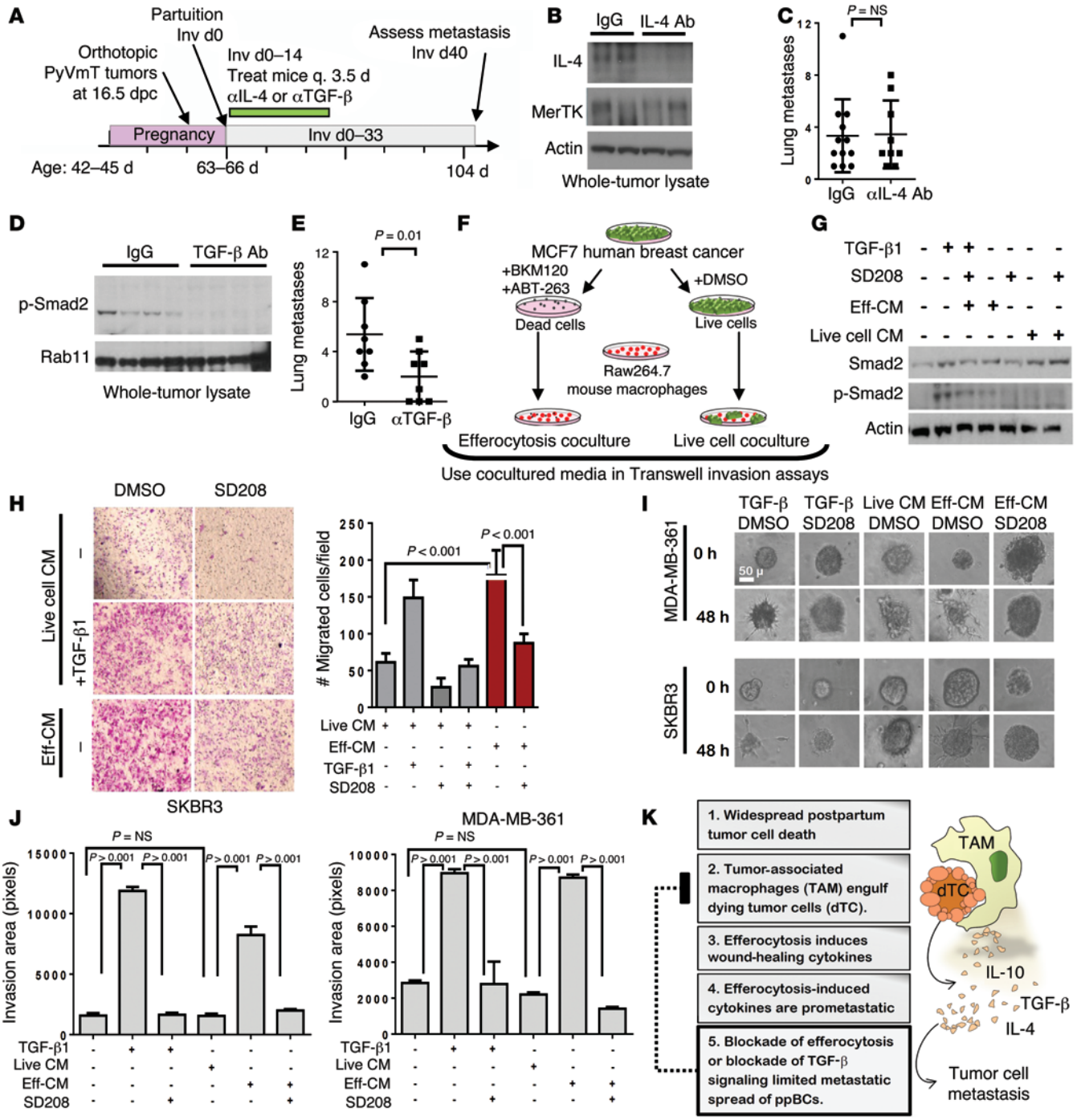

Figure 7. Postpartum TGF-β1 induction increases metastasis of ppBCs. (**A**) Postpartum mammary tumors were treated with antibodies against IL-4 (11B11) or TGF-β (1D11) twice weekly (Inv d1–14). (**B**) Western blot analysis of whole-tumor lysates 24 hours after final treatment. (**C**) Average number of lung metastases per mouse. Each point represents 1 mouse. Midline and whiskers represent the average ± SD. Student's *t* test. *n* = 9–12. (**D**) Western blot analysis of whole-tumor lysates 24 hours after final treatment. (**E**) Average number of lung metastases per mouse. Each point represents 1 mouse. Midline and whiskers represent the average ± SD. Student's *t* test. *n* = 8. (**F**) Cultured media harvested from efferocytosis cocultures and live cell cocultures were used for additional experiments. (**G**) Western blot analysis of PyVmT primary tumor cell lysates cultured in efferocytosis-conditioned, live cell–conditioned or serum-free media with or without TGF-β1 and with or without SD208. (**H**) Invasion of primary PyVmT tumor cells through Matrigel-coated Transwells in response to efferocytosis-conditioned and live cell–conditioned media over a 24-hour period. Representative images of crystal violet–stained Transwell filters are shown. Original magnification, ×40. Right panel: Average cells (± SD) invading through Matrigel-coated Transwells. (**I**) Breast cancer cell–derived spheroids were collagen embedded and overlain with live cell–conditioned, efferocytosis-conditioned, or serum-free media with or without TGF-β1 and with or without SD208. Representative images of spheroids at 0 and 24 hours after embedding per treatment are shown. Original magnification, ×400. (**J**) Average invasion area ± SD. *n* = 8–10. Student's *t* test. (**K**) Schematic model of how efferocytosis contributes to cytokine modulation and metastasis in ppBCs. Eff-CM, efferocytosis–conditioned media.

Methods

Mice. All mice were inbred on an FVB background for more than 10 generations. WT FVB, *MMTV PyVmT* and *MerTK*$^{-/-}$ mice (67), originally referred to as *Mer*^{KD}, were purchased from The Jackson Laboratory. Mice were genotyped by PCR of genomic DNA as previously described (30). Female virgin mice were randomized into 2 groups: (a) 1 group that remained virgin, and (b) 1 group that was bred from 42 to 44 days of age with WT male mice. Pregnancies were timed according to identification of a vaginal semen plug, indicating 0.5 dpc. PyVmT primary mammary tumor cells harvested from *MMTV PyVmT* polyclonal tumors (previously described in ref. 68) were collected by trypsinization, suspended 1:1 in growth factor–reduced Matrigel, and 1×10^6 cells were injected into the inguinal mammary fat pads of 57- to 59-day-old virgin or pregnant (14.5–16.5 dpc) WT female mice. *MMTV PyVmT* mice were bred with *MerTK*$^{-/-}$ mice to generate *MerTK*$^{+/+}$ *PyVmT* and *MerTK*$^{-/-}$ *PyVmT* mice. Mice were monitored daily for tumor formation by manual palpation. Pups were withdrawn at partuition to initiate involution, such that partuition was deemed Inv d0. Mice were maintained until no longer than 104 days of age, corresponding to Inv d40. In some cases, mice were treated by oral gavage with BMS-777607 (Selleck Chemicals) once daily for 7 days at 50 mg/kg in 50 μl of 0.1% Tween 80 and 0.5% methylcellulose. Where indicated in the figures, mice were treated twice weekly with 11B11 or 1D11 or isotype-matched IgGs (10 mg/kg) for 2 weeks beginning at Inv d0. 1D11 (HB-9849) and 11B11 (HB-188) were purchased from ATCC. Hybridomas were cultured, and antibodies were harvested and purified by the Vanderbilt Antibody and Protein Shared Resource.

Western analysis, immunoprecipitation, and cytokine antibody arrays. Cells and tissues were homogenized in ice-cold lysis buffer (50 mM Tris, pH 7.4, 100 mM NaF, 120 mM NaCl, 0.5% NP-40, 100 μM Na_3VO_4, 1X protease inhibitor cocktail [Roche]), sonicated for 10 seconds, and cleared by centrifugation at 4°C, 13,000 *g* for 5 minutes. Protein concentration was determined using the BCA Protein Assay (Pierce Biotechnology). Proteins were separated by SDS-PAGE, transferred to nitrocellulose membranes, blocked in 3% gelatin in TBS-T (Tris-buffered saline, 0.1% Tween 20), incubated in primary antibody overnight and in HRP-conjugated anti-rabbit or anti-mouse for 1 hour, and developed using ECL substrate (Pierce Biotechnology). The following primary antibodies were used: MerTK (α-actin, 1:10,000; Sigma-Aldrich); AKT and S473 P-Akt (1:2,000 and 1:500, respectively; Cell Signaling Technology); S6 and P-S6 (1:1,000; Cell Signaling Technology); Rab11 (1:1,000; Cell Signaling Technology). Immunoprecipitation of MerTK from 1 mg protein lysate or cell lysate was performed using goat anti-mouse MerTK antibody (R&D Systems). For cytokine arrays, whole-tumor lysates were collected and cytokine levels assayed as outlined in the mouse cytokine C1000 (8) antibody array protocol (RayBiotech). Relative cytokine levels were quantified using ImageJ software (NIH).

Histological analysis, IHC, and immunofluorescence. Tumors and mammary glands were fixed in 10% formalin (VWR Scientific), paraffin-embedded, sectioned (5 μm), and stained with H&E at the Vanderbilt University Medical Center Translational Pathology Shared Resource. IHC using rabbit antibodies against PCNA (FL-261, diluted 1:200) or arginase 1 (N-20, diluted 1:100) was performed as previously described (69) and developed using the Vectastain kit (Vector Laboratories). TUNEL analysis was performed with the TUNEL kit (Millipore). Immunofluorescence staining was performed with the following antibodies in 12% fraction V BSA (RPI Corp.): CK8 1:500 (RDI, Fitzgerald); F4/80 1:100 (Invitrogen); and goat anti-hamster and anti-rabbit 1:200 (Molecular Probes, Life Technologies). Slides were mounted in SlowFade with DAPI (Molecular Probes, Life Technologies).

qRT-PCR. Whole-tumor RNA was harvested with an RNeasy kit (QIAGEN), and cDNA was synthesized (High Capacity; Applied Biosystems) and amplified using the murine cDNA-specific primers (Integrated DNA Technologies) listed in Supplemental Methods, along with SYBR Green Supermix (Bio-Rad). The following primers were used: *MRC1* (forward: 5′ CCCTCAGCAAGCGATGTGC 3′; reverse: 5′-GGATACTTGCCAGGT CCCCA-3′); *iNOS* (forward: 5′-GGAGCATCCCAAGTACGAGTGG-3′; reverse: 5′-CGGCCCACTTCCTCCAG); *IL10* (forward: 5′-GGCGCTGTCATCGATTTCTCC; reverse: 5′-GGCCTTGTAGACACCTTGGTC); *Tgfb1* (forward: 5′-CGCAACAACGCCATCTATGAG; reverse: 5′-CGGGACAGCAATGGGGGTTC); *IL4* (forward: 5′-GGTCACAGGAGAAGGGACG; reverse: 5′-GCGAAGCACCTTGGAAGCC);, *IL12b* (forward: 5′-GGAGTGGGATGTGTCCTCAG; reverse: 5′-CGGGAGTCCAGTCCACCTCT); *CCL3* (forward: 5′-CCACTGCCCTTGCTGTTCTTCTCT; reverse: 5′-GGGTGTCAGCTCCATATGGCG); and *Rplp0* (forward: 5′-TCCTATAAAAGGCACACGCGGGC; reverse: 5′-AGACGATGTCACTCCAACGAGGACG). Target gene Ct values were normalized to mRplp0 (housekeeping gene) Ct values according to the formula: $(Ct_{\underline{target\ gene}}\text{-}Ct_{Rplp0})_{Sample\ A} - (Ct_{target\ gene}\text{-}Ct_{Rplp0})_{Sample\ B}$. Values were analyzed as the mean in fold differences (± SE, $n = 4$).

Macrophage, ACs, and efferocytosis coculture assay. PyVmT primary mammary tumor cells and MCF7 human breast cancer cells (ATCC) were transduced with viral particles (Ad.mCherry [Vector Biolabs], Ad.HSV-TK (70), or pBABE-GFP [10668; Addgene], and pLL5.0-LoxP-mCherry [Gateway]) at 5×10^9 particle-forming units per milliliter. Raw264.7 mouse macrophage cells (ATCC) were transduced with pBMN-GFP. Where indicated in the figures, cells were treated with gancyclovir (Sigma-Aldrich). To generate apoptotic MCF7, cells were treated in suspension with 1 μm BKM120 plus 2 μm ABT-263 (both inhibitors from Selleck Chemicals) for 4 hours, washed 5 times with PBS to remove residual drug, and used directly for efferocytosis assays or for annexin V staining. For efferocytosis coculture assays, Raw264.7-GFP cells (10^4/well) and PyVmT or MCF7 cells (72 hours after infection with Ad.mCherry and Ad.HSV-TK) were seeded together in a monolayer in 24-well plates in 2% FBS and cultured for 24 hours prior to the addition PBS or gancyclovir. Cells were imaged at 8, 16, and 32 h after addition of gancyclovir. Cells were collected and counted under fluorescence after 32 hours of coculture. In some experiments, Raw264.7-GFP cells (10^4/well) were seeded in a monolayer in 24-well plates and cultured for 24 hours prior to the addition of 10^3 live MCF7-mCherry or 10^3 dead MCF7-mCherry cells in serum-free media. Where indicated in the figures, BMS-777607 (1 μm) or a neutralizing goat anti-mouse MerTK antibody (AF591, 25 μg/ml; R&D Systems) (44) was added 2 hours prior to the addition of gancyclovir or 2 hours prior to the addition of dead MCF7 cells to macrophage monolayers. Live and dead MCF7 cells were similarly seeded without Raw264.7 cells as single cultures. Media were collected after 16 hours of coculture, passed through a 0.2-μm filter, and used neat (250 μl) to quantify murine IL-10 and IL-4 by ELISA (BioLegend) according to the manufacturer's protocol. Total remaining cells were collected after 16 hours of coculture, lysed, and RNA was collected using an RNeasy kit (QIAGEN).

Collagen invasion assay. MDA-MB-361 and SKBR3 cells were purchased from ATCC and used at low passage. Single-cell suspensions of cells (1×10^5) were cultured in low-adhesion plates (Corning Inc.) for 7 days in serum-free media supplemented with insulin and hydrocortisone to generate spheroids, which were transferred to collagen type I (2.5 mg/ml; Invitrogen), and collagen gels were polymerized according to the manufacturer's directions. Collagen matrices were overlain with uncultured media with or without TGF-β1 (2 pM) and with or without the TRI inhibitor SD208 (1 μM), or with cultured media harvested from Raw264.7 macrophages cocultured with either live cells (live cell–cocultured media) or dead cells (efferocytosis-cultured media) with or without SD-208. Spheroids were photographed immediately (t = 0 hours) and again after 24 hours of culture. The area of each colony at each time point was measured in pixels using Olympus DP2 software. The area at 0 hours was subtracted from the area at 24 hours to obtain the invasion area of the colony over the 24-hour period.

Statistics. All statistical analysis was carried out using GraphPad Prism software. Kaplan-Meier tumor-free survival analysis was used to assess tumor latency. One-way ANOVA or an unpaired 2-tailed Student's t test, with a 95% confidence interval, was used to determine significance for all other data. A P value less than 0.05 was considered significant.

Study approval. Mice were maintained in AAALAC-approved animal facilities at Vanderbilt University. The protocols performed herein were reviewed and approved by the IACUC of Vanderbilt University.

Acknowledgments

This work was supported by grants from the NIH (R01 CA143126, to R.S. Cook), the Vanderbilt-Ingram Cancer Center (VICC) Breast Cancer Specialized Program of Research Excellence (SPORE) (P50 CA98131, to R.S. Cook), and the Congressionally Directed Medical Research Program-Breast Cancer Research Program (CDMRP-BCRP) Idea Award (BC120793, to R.S. Cook).

Address correspondence to: Rebecca S. Cook, Vanderbilt University School of Medicine, Vanderbilt Ingram Cancer Center, Department of Cancer Biology, 2220 Pierce Ave., 759 PRB, Nashville, Tennessee 37232, USA. Phone: 615.936.3813; E-mail: rebecca.cook@vanderbilt.edu.

1. Innes KE, Byers TE. First pregnancy characteristics and subsequent breast cancer risk among young women. *Int J Cancer*. 2004; 112(2):306–311.
2. Pathak DR. Dual effect of first full term pregnancy on breast cancer risk: empirical evidence and postulated underlying biology. *Cancer Causes Control*. 2002;13(4):295–298.
3. Lyons TR, Schedin PJ, Borges VF. Pregnancy and breast cancer: when they collide. *J Mammary Gland Biol Neoplasia*. 2009;14(2):87–98.
4. Martinson HA, Lyons TR, Giles ED, Borges VF, Schedin P. Developmental windows of breast cancer risk provide opportunities for targeted chemoprevention. *Exp Cell Res*. 2013; pii(11):S0014-4827(13)00189-4.
5. Schedin P. Pregnancy-associated breast cancer and metastasis. *Nat Rev Cancer*. 2006; 6(4):281–291.
6. Schedin PJ, Watson CJ. The complexity of the relationships between age at first birth and breast cancer incidence curves implicate pregnancy in cancer initiation as well as promotion of existing lesions. Preface. *J Mammary Gland Biol Neoplasia*. 2009;14(2):85–86.
7. Callihan EB, et al. Postpartum diagnosis demonstrates a high risk for metastasis and merits an expanded definition of pregnancy-associated breast cancer. *Breast Cancer Res Treat*. 2013;138(2):549–559.
8. Faupel-Badger JM, et al. Postpartum remodeling, lactation, and breast cancer risk: summary of a National Cancer Institute-sponsored workshop. *J Natl Cancer Inst*. 2013;105(3):166–174.
9. Amant F, et al. Prognosis of women with primary breast cancer diagnosed during pregnancy: results from an international collaborative study. *J Clin Oncol*. 2013;31(20):2532–2539.
10. Lyons TR, et al. Postpartum mammary gland involution drives progression of ductal carcinoma in situ through collagen and COX-2. *Nat Med*. 2011;17(9):1109–1115.
11. McDaniel SM, et al. Remodeling of the mammary microenvironment after lactation promotes breast tumor cell metastasis. *Am J Pathol*. 2006;168(2):608–620.
12. Schedin P, O'Brien J, Rudolph M, Stein T, Borges V. Microenvironment of the involuting mammary gland mediates mammary cancer progression. *J Mammary Gland Biol Neoplasia*. 2007;12(1):71–82.
13. O'Brien J, Schedin P. Macrophages in breast cancer: do involution macrophages account for the poor prognosis of pregnancy-associated breast cancer? *J Mammary Gland Biol Neoplasia*. 2009;14(2):145–157.
14. O'Brien JH, Vanderlinden LA, Schedin PJ, Hansen KC. Rat mammary extracellular matrix composition and response to ibuprofen treatment during postpartum involution by differential GeLC-MS/MS analysis. *J Proteome Res*. 2012;11(10):4894–4905.
15. Schedin P, Borges V. Breaking down barriers: the importance of the stromal microenvironment in acquiring invasiveness in young women's breast cancer. *Breast Cancer Res*. 2009;11(2):102.
16. O'Brien J, et al. Alternatively activated macrophages and collagen remodeling characterize the postpartum involuting mammary gland across species. *Am J Pathol*. 2010;176(3):1241–1255.
17. Fornetti J, Jindal S, Middleton KA, Borges VF, Schedin P. Physiological COX-2 expression in breast epithelium associates with COX-2 levels in ductal carcinoma in situ and invasive breast cancer in young women. *Am J Pathol*. 2014;184(4):1219–1229.
18. Ruffell B, Affara NI, Coussens LM. Differential macrophage programming in the tumor microenvironment. *Trends Immunol*. 2012;33(3):119–126.
19. Qian BZ, Pollard JW. Macrophage diversity enhances tumor progression and metastasis. *Cell*. 2010;141(1):39–51.
20. Coussens LM, Zitvogel L, Palucka AK. Neutralizing tumor-promoting chronic inflammation: a magic bullet? *Science*. 2013;339(6117):286–291.
21. Denardo DG, et al. Leukocyte complexity predicts breast cancer survival and functionally regulates response to chemotherapy. *Cancer Discov*. 2011;1(1):54–67.
22. Tlsty TD, Coussens LM. Tumor stroma and regulation of cancer development. *Annu Rev Pathol*. 2006;1:119–150.
23. Balkwill F, Charles KA, Mantovani A. Smoldering and polarized inflammation in the initiation and promotion of malignant disease. *Cancer Cell*. 2005;7(3):211–217.
24. Kristensen VN, et al. Integrated molecular profiles of invasive breast tumors and ductal carcinoma in situ (DCIS) reveal differential vascular and interleukin signaling. *Proc Natl Acad Sci U S A*. 2012;109(8):2802–2807.
25. Faghih Z, Erfani N, Haghshenas MR, Safaei A, Talei AR, Ghaderi A. Immune profiles of $CD4^+$ lymphocyte subsets in breast cancer tumor draining lymph nodes. *Immunol Lett*. 2014;158(1):57–65.
26. Clarkson RW, Wayland MT, Lee J, Freeman T, Watson CJ. Gene expression profiling of mammary gland development reveals putative roles for death receptors and immune mediators in post-lactational regression. *Breast Cancer Res*. 2004;6(2):R92–109.
27. Asztalos S, et al. Gene expression patterns in the human breast after pregnancy. *Cancer Prev Res (Phila)*. 2010;3(3):301–311.
28. Stein T, Salomonis N, Nuyten DS, van de Vijver MJ, Gusterson BA. A mouse mammary gland involution mRNA signature identifies biological pathways potentially associated with breast cancer metastasis. *J Mammary Gland Biol Neoplasia*. 2009;14(2):99–116.
29. Flanders KC, Wakefield LM. Transforming growth factor-(beta)s and mammary gland involution; functional roles and implications for cancer progression. *J Mammary Gland Biol Neoplasia*. 2009;14(2):131–144.
30. Sandahl M, Hunter DM, Strunk KE, Earp HS,

Cook RS. Epithelial cell-directed efferocytosis in the post-partum mammary gland is necessary for tissue homeostasis and future lactation. *BMC Dev Biol*. 2010;10:122.
31. Cook RS, et al. MerTK inhibition in tumor leukocytes decreases tumor growth and metastasis. *J Clin Invest*. 2013;123(8):3231–3242.
32. Guy CT, Cardiff RD, Muller WJ. Induction of mammary tumors by expression of polyomavirus middle T oncogene: a transgenic mouse model for metastatic disease. *Mol Cell Biol*. 1992;12(3):954–961.
33. Kreuzaler PA, et al. Stat3 controls lysosomal-mediated cell death in vivo. *Nat Cell Biol*. 2011;13(3):303–309.
34. Seitz HM, Camenisch TD, Lemke G, Earp HS, Matsushima GK. Macrophages and dendritic cells use different Axl/Mertk/Tyro3 receptors in clearance of apoptotic cells. *J Immunol*. 2007;178(9):5635–5642.
35. Zizzo G, Hilliard BA, Monestier M, Cohen PL. Efficient clearance of early apoptotic cells by human macrophages requires M2c polarization and MerTK induction. *J Immunol*. 2012;189(7):3508–3520.
36. Schroeder GM, et al. Discovery of N-(4-(2-amino-3-chloropyridin-4-yloxy)-3-fluorophenyl)-4-ethoxy-1-(4-fluorophenyl)-2-oxo-1,2-dihydropyridine-3-carboxamide (BMS-777607), a selective and orally efficacious inhibitor of the Met kinase superfamily. *J Med Chem*. 2009;52(5):1251–1254.
37. Stein T, et al. Involution of the mouse mammary gland is associated with an immune cascade and an acute-phase response, involving LBP, CD14 and STAT3. *Breast Cancer Res*. 2004;6(2):R75–R91.
38. Wallet MA, et al. MerTK is required for apoptotic cell-induced T cell tolerance. *J Exp Med*. 2008;205(1):219–232.
39. Lemke G, Burstyn-Cohen T. TAM receptors and the clearance of apoptotic cells. *Ann N Y Acad Sci*. 2010;1209:23–29.
40. Rothlin CV, Ghosh S, Zuniga EI, Oldstone MB, Lemke G. TAM receptors are pleiotropic inhibitors of the innate immune response. *Cell*. 2007;131(6):1124–1136.
41. Clarkson RW, Watson CJ. Microarray analysis of the involution switch. *J Mammary Gland Biol Neoplasia*. 2003;8(3):309–319.
42. Watson CJ. Immune cell regulators in mouse mammary development and involution. *J Anim Sci*. 2009;87(13):35–42.
43. Teschendorff AE, et al. Improved prognostic classification of breast cancer defined by antagonistic activation patterns of immune response pathway modules. *BMC Cancer*. 2010;10:604.
44. Park HJ, Baen JY, Lee YJ, Choi YH, Kang JL. The TAM-family receptor Mer mediates production of HGF through the RhoA-dependent pathway in response to apoptotic cells. *Mol Biol Cell*. 2012;23(16):3254–3265.
45. O'Brien J, Martinson H, Durand-Rougely C, Schedin P. Macrophages are crucial for epithelial cell death and adipocyte repopulation during mammary gland involution. *Development*. 2012;139(2):269–275.
46. Hughes K, Wickenden JA, Allen JE, Watson CJ. Conditional deletion of Stat3 in mammary epithelium impairs the acute phase response and modulates immune cell numbers during post-lactational regression. *J Pathol*. 2012;227(1):106–117.
47. Vandivier RW, Henson PM, Douglas IS. Burying the dead: the impact of failed apoptotic cell removal (efferocytosis) on chronic inflammatory lung disease. *Chest*. 2006;129(6):1673–1682.
48. deCathelineau AM, Henson PM. The final step in programmed cell death: phagocytes carry apoptotic cells to the grave. *Essays Biochem*. 2003;39:105–117.
49. Erwig LP, Henson PM. Clearance of apoptotic cells by phagocytes. *Cell Death Differ*. 2008;15(2):243–250.
50. Thorp E, Subramanian M, Tabas I. The role of macrophages and dendritic cells in the clearance of apoptotic cells in advanced atherosclerosis. *Eur J Immunol*. 2011;41(9):2515–2518.
51. Fullerton JN, O'Brien AJ, Gilroy DW. Pathways mediating resolution of inflammation: when enough is too much. *J Pathol*. 2013;231(1):8–20.
52. Fadok VA, Voelker DR, Campbell PA, Cohen JJ, Bratton DL, Henson PM. Exposure of phosphatidylserine on the surface of apoptotic lymphocytes triggers specific recognition and removal by macrophages. *J Immunol*. 1992;148(7):2207–2216.
53. Fadok VA, Bratton DL, Konowal A, Freed PW, Westcott JY, Henson PM. Macrophages that have ingested apoptotic cells in vitro inhibit proinflammatory cytokine production through autocrine/paracrine mechanisms involving TGF-β, PGE2, and PAF. *J Clin Invest*. 1998;101(4):890–898.
54. Filardy AA, et al. Proinflammatory clearance of apoptotic neutrophils induces an IL-12(low) IL-10(high) regulatory phenotype in macrophages. *J Immunol*. 2010;185(4):2044–2050.
55. Huynh ML, Fadok VA, Henson PM. Phosphatidylserine-dependent ingestion of apoptotic cells promotes TGF-beta1 secretion and the resolution of inflammation. *J Clin Invest*. 2002;109(1):41–50.
56. DeNardo DG, et al. CD4(+) T cells regulate pulmonary metastasis of mammary carcinomas by enhancing protumor properties of macrophages. *Cancer Cell*. 2009;16(2):91–102.
57. Gong D, Shi W, Yi SJ, Chen H, Groffen J, Heisterkamp N. TGFβ signaling plays a critical role in promoting alternative macrophage activation. *BMC Immunol*. 2012;13:31.
58. Wan E, et al. Enhanced efferocytosis of apoptotic cardiomyocytes through myeloid-epithelial-reproductive tyrosine kinase links acute inflammation resolution to cardiac repair after infarction. *Circ Res*. 2013;113(8):1004–1012.
59. Choi JY, et al. Upregulation of Mer receptor tyrosine kinase signaling attenuated lipopolysaccharide-induced lung inflammation. *J Pharmacol Exp Ther*. 2013;344(2):447–458.
60. Kazeros A, Harvey BG, Carolan BJ, Vanni H, Krause A, Crystal RG. Overexpression of apoptotic cell removal receptor MERTK in alveolar macrophages of cigarette smokers. *Am J Respir Cell Mol Biol*. 2008;39(6):747–757.
61. Gautier EL, et al. Gene-expression profiles and transcriptional regulatory pathways that underlie the identity and diversity of mouse tissue macrophages. *Nat Immunol*. 2012;13(11):1118–1128.
62. Patin E, et al. Genome-wide association study identifies variants associated with progression of liver fibrosis from HCV infection. *Gastroenterology*. 2012;143(5):1244–1252.
63. Loges S, et al. Malignant cells fuel tumor growth by educating infiltrating leukocytes to produce the mitogen Gas6. *Blood*. 2010;115(11):2264–2273.
64. Linger RM, et al. Mer or Axl receptor tyrosine kinase inhibition promotes apoptosis, blocks growth and enhances chemosensitivity of human non-small cell lung cancer. *Oncogene*. 2013;32(29):3420–3431.
65. Whitman SP, et al. GAS6 expression identifies high-risk adult AML patients: potential implications for therapy. *Leukemia*. 2014;28(6):1252–1258.
66. Keating AK, et al. Inhibition of Mer and Axl receptor tyrosine kinases in astrocytoma cells leads to increased apoptosis and improved chemosensitivity. *Mol Cancer Ther*. 2010;9(5):1298–1307.
67. Scott RS, et al. Phagocytosis and clearance of apoptotic cells is mediated by MER. *Nature*. 2001;411(6834):207–211.
68. Cook RS, et al. ErbB3 ablation impairs PI3K/Akt-dependent mammary tumorigenesis. *Cancer Res*. 2011;71(11):3941–3951.
69. Vaught DB, et al. HER3 is required for HER2-induced preneoplastic changes to the breast epithelium and tumor formation. *Cancer Res*. 2012;72(10):2672–2682.
70. Candolfi M, et al. Release of HMGB1 in response to proapoptotic glioma killing strategies: efficacy and neurotoxicity. *Clin Cancer Res*. 2009;15(13):4401–4414.